Title

Assessing the impact of extreme climate events on European gross primary production

Authors

Zhang, Huihui

Loaiciga, Hugo A

Okujeni, Akpona

et al.

Publication Date

2025-03-01

DOI

10.1016/j.agrformet.2024.110374

Peer reviewed

Agricultural and Forest Meteorology 362 (2025) 110374

Contents lists available at ScienceDirect

Agricultural and Forest Meteorology

journal homepage: www.elsevier.com/locate/agrformet

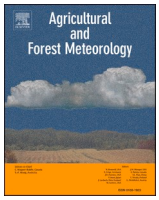

Assessing the impact of extreme climate events on European gross primary production

Huihui Zhang [a,*], Hugo A Loaiciga [b], Akpona Okujeni [a], Ji Liu [c,d], Min Tan [e], Tobias Sauter [a]

[a] Geography Department, Humboldt-Universität zu Berlin, Berlin, 12489, Germany
[b] Department of Geography, University of California, Santa Barbara, CA 93106, USA
[c] Department of Ecohydrology, Leibniz Institute of Freshwater Ecology and Inland Fisheries, Berlin, 12587, Germany
[d] Hubei Province Key Laboratory for Geographical Process Analysis and Simulation, Central China Normal University, Wuhan, 430079, China
[e] The Third Geodetic Surveying Brigade of MNR The First Serving and Mapping Engineering Institute of Sichuan Province, Chengdu, 610100, China

ARTICLE INFO

Keywords:
Gross primary production
Extreme climate events
Irrigation management
Climate regimes
Landcover types

ABSTRACT

Climate warming and the associated intensification of extreme climate events (such as droughts, heavy precipitation, and heatwaves) present challenges to plant growth. Plant growth is influenced by a number of factors such as soil moisture, water demand by plants, temperature sensitivity, growth stage, and by irrigation practices in the case of crops. The response of plant growth to extreme climate events across a range of growing periods, climate regions, and agricultural land types under different irrigation strategies remains unclear. This study utilizes ten extreme climate indices and six drought indices to predict plant growth outcomes, as indicated by the end-of-growing season Gross Primary Production (GPP), across different growing seasons in Europe from 2003 to 2020. This work examines the impact of extreme climate events on plant growth with a novel explainable LightGBM model. This model elucidates the contribution of such events to plant growth, and helps to identify their tipping points. This paper's results demonstrate that early-season soil moisture and extreme absolute temperatures are key predictors in forecasting the end-of-growing season GPP, indicating potential drought memory. Plant growth correlates highly with extreme climate events in arid, cold, and temperate climates. In arid climates the extreme precipitation amounts are the predominant predictor of end-of-growing season GPP. Agricultural drought plays a leading role in the model prediction results in cold climates. Extreme climate events have a more pronounced effect on plant growth yield in rainfed cropland and grasslands compared to irrigated croplands. The implementation of irrigation strategies involving human intervention would help mitigate the impact of extreme climate events on plant growth outcomes.

1. Introduction

Climate change causes extreme climate events in many regions, and extreme climate events (e.g., droughts, heavy precipitation, and heatwaves) reduce crop yields and impact various economic sectors (Chiang et al., 2021; Krishnamurthy et al., 2022; Rezaei et al., 2023). The average annual economic loss due to extreme climate events was approximately 9 billion euros in Europe from 1981 to 2010, with half of these losses originating from agriculture (Jin et al., 2023). Crop losses are expected to increase to more than 65 billion euros per year if no climate mitigation measures are taken, i.e. a 4 °C rise in surface temperature by 2100 (Naumann et al., 2021).

Since the second half of the 20th century extreme climate conditions in Europe have intensified (Frich et al., 2002; Ebi and Bowen, 2016). Recent studies have shown that precipitation- and temperature-related extreme events have various effects on plant growth (Dai et al., 2018; Teshome and Zhang, 2019; Sun et al., 2021; Rezaei et al., 2023). Flooding and waterlogging triggered by extreme precipitation may cause direct damage to plant growth and influence the efficiency of photosynthesis (Chen et al., 2023). The sensitivity of photosynthesis to extreme precipitation depends on the frequency, intensity, and duration of precipitation events (Li et al., 2019). Heatwaves stemming from extreme temperatures also limit plant growth. A European mega heatwave in 2003 led to a drought that resulted in a 30% loss of gross primary production (Ciais et al., 2005; Niu et al., 2014). The lack of precipitation, elevated temperatures, and reduced soil moisture

* Corresponding author.
E-mail address: huihui.zhang@geo.hu-berlin.de (H. Zhang).

https://doi.org/10.1016/j.agrformet.2024.110374
Received 20 March 2024; Received in revised form 2 December 2024; Accepted 18 December 2024
Available online 26 December 2024

impacted the morphological, physiological, and biochemical plant processes (Gulzar and Mazumder, 2023).

Droughts are broadly categorized into four types: meteorological, agricultural, hydrological, and socioeconomic (Wilhite and Glantz, 1985). Previous studies proposed that meteorological and agricultural drought play a significant role in plant growth (Kuśmierek-Tomaszewska and Żarski, 2021). Meteorological drought is typically the precursor to other types of droughts, characterized by a prolonged lack of precipitation leading to an overall soil moisture deficit (Xu et al., 2021; Zhang et al., 2023a). External environmental factors control the soil moisture deficit in the shallow soil and root zone, which regulates plant function. This type of drought is referred to as agricultural drought (Krueger et al., 2019, McCormick et al., 2021).

Understanding the role of extreme climate events on plant growth and harvest losses is key in disaster prevention and food security. The overall effect on plant growth is measured by the Gross Primary Production (GPP). Previous studies have indeed shown that extreme climate events lead to abnormally low yield results, but they often neglect the complex interaction of multiple extreme climate events on plant growth which occurs at all growth stages of plants (Feng et al., 2021; Leng and Hall, 2019). This ultimately leads to yield reduction and harvest loss (Zhang et al., 2023b). Until present the role of extreme climate events in predicting plant growth in different growing periods has remained unclear. A first step in this direction was taken by Chatterjee et al. (2022), who considered the role of meteorological and agricultural drought in plant growth in the United States (CONUS). However, the evaluation is limited to recent years due to insufficient soil moisture gauge stations and monitoring satellites (e.g., Soil Moisture Active Passive (SMAP) data have been available only since 2015). Previous studies have ignored the cross-cutting effects of multiple extreme weather events, such as droughts, heat waves, and heavy precipitation. Other studies faced similar problems and restricted their analysis to the specific type of extreme climate events (Peng et al., 2011; Islam et al., 2021). Moreover, the effects of extreme climate events on plant growth may vary significantly with different climate regimes, landcover (LC) types, and irrigation management types. For example, in arid regions, infiltration rates sometimes are relatively low, especially in summer, due to crust formation on the soil surface. The reduced infiltration can lead to flooding during extreme precipitation events, as water accumulates on the surface instead of seeping into the ground. Additionally, high evaporative losses from the topsoil further reduce the availability of moisture for infiltration (Tugwell-Wootton et al. 2020). In temperate regions, where potential evapotranspiration only slightly exceeds rainfall and rain events are typically large, extreme rain events are likely to be less important for driving plant growth. This is because much of the rainfall from extreme events may be lost to runoff or deep infiltration below the root zone, or it may exceed the capacity of plants to uptake it (O'Donnell et al., 2021).

The primary aim of this study is to enhance our understanding of the interactions between different extreme climate events and plant growth at the continental level, encompassing various climate regimes, LC, and irrigation management types, particularly on agricultural land. Specifically, this work evaluates the effects of extreme climate events on plant growth using an explainable machine learning method. The model predicts the end-of-growing season GPP in Europe in the period 2003 to 2020. This study examines the impact of extreme climate events (droughts, extreme precipitation, and heatwaves) on plant growth, quantifies the sensitivity of plant growth during various growth periods to extreme events, and assesses the impact on GPP. These research questions are explored across three climate regions (cold, temperate, and arid) and three types of agricultural lands (grassland, irrigated croplands, and rainfed croplands).

This study furthers our understanding of the impacts of extreme climate events during various growth periods of plants, and improves our understanding of the predominant roles of different extreme climate events across various climate regimes and agricultural lands.

2. Methods and materials

This study examines the complex interaction between extreme climate events and plant growth, focusing specifically on agricultural land. Models were run only for pixels identified as one of three agricultural land types, i.e. grassland, irrigated croplands, and rainfed croplands. Our analytical approach is detailed in Fig. 1. Extreme climate indices and drought indices are used to describe the occurrence of extreme climate events and quantify the severity of drought conditions, specifically related to precipitation, temperature, and soil moisture. Ten extreme climate indices and six classical drought indices are applied as potential predictors. GPP measures vegetation growth and is an indicator of global food production, serving as a proxy for plant growth in this study (Li et al.,2022). An explainable ML model predicts the end-of-growing season GPP. The relative contributions of extreme events on different growth periods, land use types, and climate regions are quantified using the SHapley Additive exPlanations (SHAP) algorithm.

2.1. Remote sensing data, extreme climate indices, and drought indices

Ten extreme climate indices are derived from the E-OBS daily precipitation and temperature dataset (Cornes et al., 2018; Haylock et al., 2008). Six drought indices are derived from SoMo.ml-EU, GSSM1 km, SoilGrids250m, E-OBS, MODIS ET, and PET datasets. All the satellite products and indices used in this study were rescaled to a 10 km grid over Europe and aggregated to 16 days from their original temporal resolution to maintain consistency with the GPP dataset. Tables 1 and Table 2 show the datasets and extreme climate indices used in this study, while Table 3 shows the six drought indices. A detailed description of data acquisition, the preprocessing of remote sensing products, extreme climate indices, and drought indices, is given in the Supplementary Information.

Extreme climate indices summarize aspects of the distribution of climate variables (e.g., temperature and precipitation), with a focus on extreme conditions (Zhang et al., 2011). Precipitation-related extreme climate indices provide a numerical representation of flooding and heavy precipitation events. Temperature-related extreme climate indices offer a quantitation description of heatwaves. Anomalies in soil moisture and atmospheric drivers are usually assessed by drought indices (Heim, 2002). Meteorological and agricultural drought indices rely on precipitation, evapotranspiration, and soil moisture stress to describe various degrees of drought severity.

The selected extreme climate indices include six precipitation-related metrics: Rx1day, Rx5day, R95p, CT, CDD, and CWD, and four temperature-related metrics: TNx, TN90p, TXx, and TX90p based on the Expert Team on Climate Change Detection and Indices (ETCCDI). These indices characterize precipitation events and heatwave conditions (Fischer et al.,2014; Sun et al., 2021). The set includes both absolute indices (Rx1day, Rx5day, CT, TNx, TXx, CDD, CWD) and relative indices (R95p, TN90p, TX90p) (Sheridan and Lee, 2018). Specifically, the precipitation indices Rx1day, Rx5day, and CT are used to examine the effects of instantaneous maximum precipitation and cumulative precipitation on gross primary production (GPP). Moreover, the R95p, CDD, and CWD indices are used to investigate the effect of precipitation intensity and duration on GPP. On the other hand, temperature-related indices assess the impact of extreme temperature events on GPP.

Table 3 lists the summary of meteorology/agricultural drought indices employed in this study. The assessment of plant growth in agricultural studies is commonly linked to meteorological and agricultural drought. This paper investigates the impact of different drought categories (meteorological, agricultural, or hybrid agricultural and meteorological drought) on plant growth. Additionally, soil moisture plays a vital role in linking drought, climate, and vegetation, primarily consisting of surface soil moisture (held in the top 0–5 cm of soil) and root zone soil moisture (held in the 0–50 cm layer of soil) (O et al.,

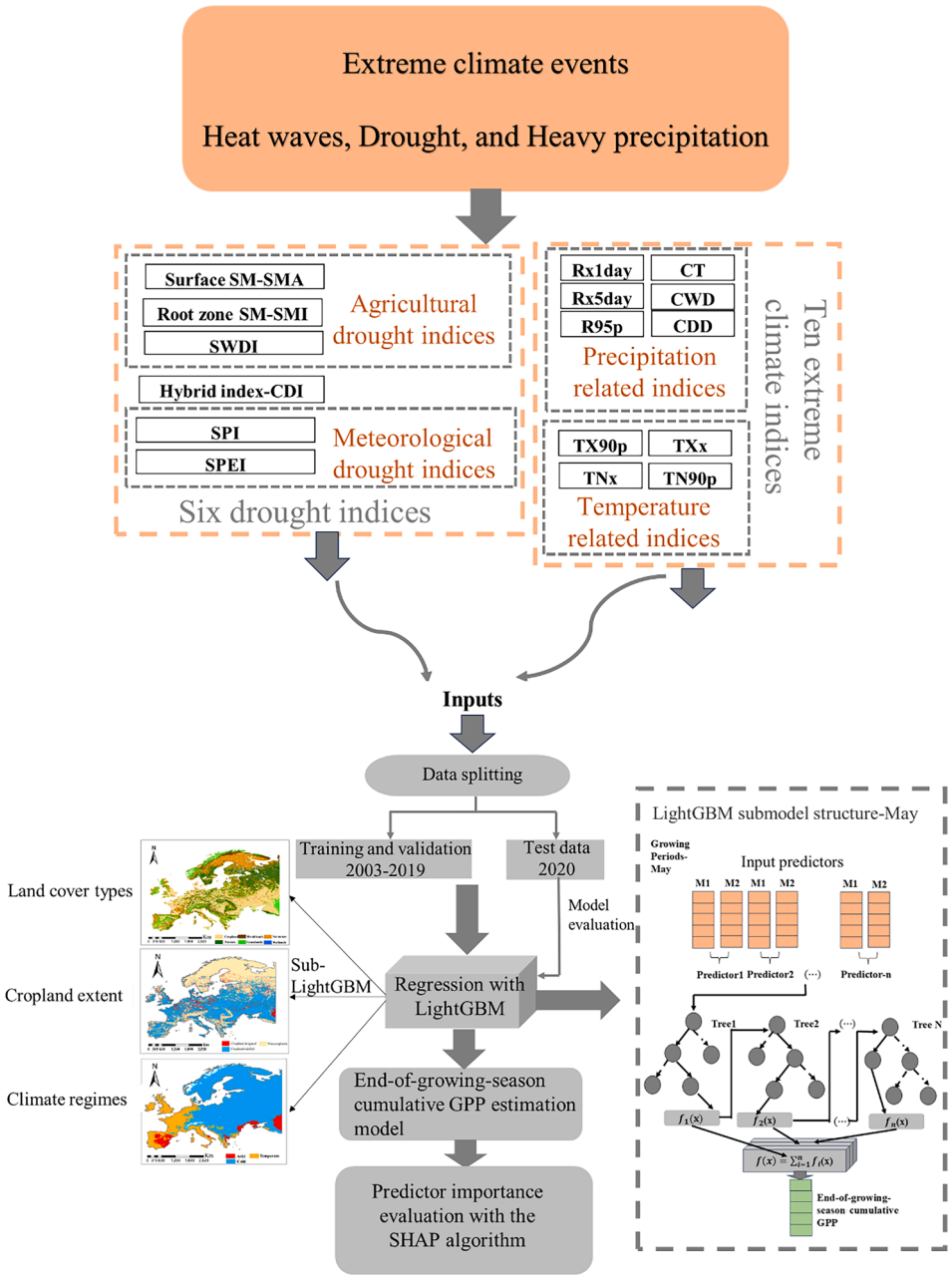

Fig. 1. Methodology of the study. Acronyms and descriptions of indices are given in Tables 2 and 3. Note: M1 and M2 refer to early May (about the 9th day) and late May (about the 25th day), respectively. Submodel "M" is presented as an example corresponding to the growing period in May.

2022). Agricultural drought is characterized by soil moisture, with root zone soil moisture and surface soil moisture used to calculate agricultural drought indices, respectively. Six drought indices are considered, including three agricultural drought indices (i.e., the surface soil moisture (0–5 cm) product-based index-SMA, the root zone soil moisture (0–50 cm) product-based index-SMI, and the Soil Water Deficit Index (SWDI)), and two meteorological drought indices (i.e., the standardized precipitation index (SPI) and the standardized precipitation evapotranspiration index (SPEI)). In addition, a hybrid index combining meteorological and agricultural drought, named the Comprehensive Drought Index (CDI), is included. The CDI is used to assess whether a combined index provides a better description of plant growth conditions than soil moisture or atmospheric indices alone (Chatterjee et al., 2022). The study area is displayed in Fig. S1. The historical crop yields are applied to verify the correlation between GPP and major crop yields in Europe (see Supplementary Fig. S4).

2.2. *Forecasting end-of-growing season GPP based on extreme climate events*

The explainable LightGBM model was used to disentangle the role that extreme climate events have on plant growth. This model has been widely used in environmental meteorology and considerably outperforms eXtreme Gradient Boosting and stochastic gradient boosting in terms of computational speed and memory requirements (Ma et al., 2022; Xu et al., 2023; Yu et al., 2023). This study evaluates the LightGBM model's prediction of end-of-growing season GPP using predictors listed in Tables 2 and 3 (i.e., extreme climate indices and drought indices) derived from different periods of growing seasons. This work focuses on the growing season from early May to mid-October for the years 2003–2020 to avoid frozen soil conditions. The predictors were aggregated on a 16-day basis. The choice of a 16-day temporal scale aims to capture the impacts of short-range extreme climate events on

Table 1
Description of the datasets.

Dataset	Variables	Original spatial resolution	Original temporal resolution	Period	Reference
E-OBS dataset	Precipitation Minimum temperature Maximum temperature	0.1°(~10 km)	1 day	2003–2020	Cornes et al. (2018)
MODIS ET	Actual evapotranspiration	500 m	8 day	2003–2020	Running et al. (2017)
MODIS PET	Potential evapotranspiration	500 m	8 day	2003–2020	Running et al. (2017)
MODIS GPP	Gross primary production	500 m	8 day	2003–2020	Running et al. (2015)
MODIS Landcover	Landcover maps	500m	1 year	2020	Friedl and Sulla-Menashe (2022)
GFSAD Cropland Extent map	Irrigated and rainfed cropland maps	1 km	/	2010	Teluguntla et al. (2015)
Climate	Koppen-Geiger climate classification map	1 km	/	1980–2016	Beck (2018)
SoMo.ml-EU	Root-zone soil moisture (0–50 cm)	0.1°(~10 km)	1 day	2003–2020	O et al. (2022)
GSSM1km	Surface soil moisture (0–5 cm)	1 km	1 day	2003–2020	Han et al. (2023)
ISRIC SoilGrids250m	FC and WP (averaged to 0–60 cm)	5 km	/	/	Hengl, et al. (2017)
GDHYv1.2+v1.3	Historical crop yields	0.5° (~50 km)	1 year	2003–2016	Iizumi and Sakai (2020)

Note: All spatial data were aggregated to a resolution of 10 km and all temporal data were aggregated to a time scale of 16-days. E-OBS - Ensembles Daily Gridded Observational Dataset in Europe; MODIS - Moderate Resolution Imaging Spectroradiometer product; GFSAD - Global Food Support Analysis Data; SoMo.ml - Machine Learning-based Soil Moisture product; GSSM1km - Global Surface Soil Moisture; ISRIC SoilGrids250m - Global Gridded Soil Information based on Machine Learning, provided by International Soil Reference and Information Centre; GDHY - Global Dataset of Historical Yield; ET - Actual Evapotranspiration; PET - Potential Evapotranspiration; FC - Field Capacity; WP - Wilting Point.

plant growth. Two 16-day periods are used in each month: one covering the first half of the month (around the 9th day) and one covering the second half (around the 25th day). This results in eleven 16-day periods for a growing season, with 198 data values for each pixel over the whole period of analysis.

The LightGBM model was fitted using a combination of extreme climate indices, drought indices, and different months (i.e., M, MJ, MJj, MJjA, MJjAS, MJjASO), where the capital letters represent the initials of the month name (i.e., May (M), June (J), August (A), September (S), and October (O)), except for July, which is denoted by "j". The different periods also represent various growth stages of the plants. Early growth seasons include May and June, while early-to-mid growth seasons encompass May to August, and the full growth seasons span from May to October. It is worth noting that this work applies individual month indices along with monthly combinations to understand if there is any possible memory of extreme climate events in forecasting GPP (i.e., plant growth). The input datasets were divided into training and validation (2003–2019, 70%:30%), and testing (year 2020) datasets. The forecast skill of the model is evaluated based on the testing dataset. The training procedure was repeated ten times with different training/validation sets for each iteration, and the average forecast accuracy was herein used for analysis.

The relationship between plant growth and extreme climate events was further evaluated across different growing periods, climate regimes, irrigation management, and agricultural LC types. The evaluation of model forecast performance is based on the statistical indices. Our ML forecast procedure is similar to previous applications (Dikshit and Pradhan, 2021; Chatterjee et al., 2022).

2.3. Statistical indices

The coefficient of determination (R^2), and root mean square error (RMSE in kg C/m^2) are used to assess the performance of the LightGBM model. In general, greater R^2 and smaller RMSE indicate relatively better model performance. It is important to note that this study focuses on investigating the cross-cutting effects of multiple predictors (extreme climate events) on predictions (GPP). Here, R^2 and RMSE are used as reference statistics to investigate the impact of predictors, rather than as absolute measures of prediction accuracy. The classic work by Anderson and Sclove (1978) provides guidelines for the interpretation of the magnitude of R^2 insofar as the linear statistical association between two variables is concerned as follows: $R^2 = 0$: there is no correlation; $R^2 = 0$ - 0.25: there is weak correlation; $R^2 = 0.25$ - 0.64 there is medium correlation; $R^2 = 0.64$ - 1: there is strong correlation; $R^2 = 1$: there is perfect correlation between two variables. The variance inflation factor (VIF) is applied to select predictors that reduce the possible impact induced by multicollinearity (Wilks, 2011) among the predictor variables, specifically those derived from two dates within a month (see Eq. 1). A VIF greater than the threshold indicates a high likelihood of multicollinearity. Variables with VIF values exceeding this threshold were systematically removed from the LightGBM model.

$$VIF = \frac{1}{1 - R_i^2} \tag{1}$$

Where R_i^2 represents the R^2 value calculated by regressing the i-th predictor variable against all the other predictor variables in the model. A VIF value of 1 indicates no correlation, while higher values suggest increasing levels of multicollinearity. In this study the VIF threshold is set at a common value, which is 10 (Franke, 2010).

2.4. Explainable artificial intelligence algorithm

Previous studies have used variable-importance diagrams to identify the most and least important predictor variables in the ML model (Khan et al., 2020). However, this approach cannot explain the contribution of second-order effects (interaction) on a given model outcome. Dikshit and Pradhan (2021) overcame this problem by implementing the SHAP method to improve the model's interpretation with respect to spatial drought forecasting (Dikshit and Pradhan, 2021; Cheng et al., 2023; Zhang et al., 2024). The SHAP method calculates the marginal contribution of each predictor instance to the model prediction (Shapley, 1953, Lundberg and Lee, 2017). The average contribution of a predictor instance among all possible coalitions is given by the SHAP value. The SHAP value is a measure of the contribution of the predictors to the final prediction. SHAP provides multiple AI model explainers, including Kernel Explainer, Deep Explainer, Tree Explainer, and Gradient Explainer. A detailed explanation of different explainers and the corresponding plot types is found in Molnar, (2020). Tree Explainer was used for outputs of the LightGBM model (Abdollahi and Pradhan, 2023). The "relevant explainer" can be used to create three graphs to facilitate interpretation of the results: (i) Summary plot; (ii) Dependence plot; and (iii) Force plot. For details of all plots see Christoph (2019). The

Table 2
Definitions of extreme climate indices.

Category	Abbreviation	Full name	Definition	Unit
Precipitation index	Rx1day	Maximum 1-day precipitation	Maximum 1-day precipitation within 16 days	mm
	Rx5day	Maximum consecutive 5-day precipitation	Maximum consecutive 5-day total precipitation within 16 days	mm
	R95p	Very wet days	16-day precipitation from days >95th percentile	mm
	CT	Maximum consecutive n days precipitation (n≤16)	Total precipitation amounts over the maximum number of consecutive days within a 16-day period	mm
	CWD	Maximum length of wet spell	Maximum Consecutive wet days with precipitation > 1 mm within a 16-day period	day
	CDD	Maximum length of dry spell	Maximum consecutive dry days with precipitation ≤1 mm within a 16-day period	day
Temperature index	TX90p	Warm days	Percentage of 16 days when daily maximum temperature >90th percentile	%
	TXx	16-day maximum value of daily maximum temperature	Maximum value of 16-day maximum temperature	%
	TN90p	Warm nights	Percentage of 16 days when daily minimum temperature >90th percentile	°C
	TNx	16-day maximum value of minimum temperature	Maximum value of 16-day minimum temperature	°C

summary plot and dependence plot are typical visualizations focusing on understanding the feature interaction effects conducted on the ML model's decision process.

3. Results

3.1. Overall performance

The model prediction accuracy for the six growing periods was analyzed with individual precipitation-related extreme climate indices, temperature-related extreme climate indices, and drought indices and are shown in Fig. 2. Table 4 and Fig. 3 show the forecast accuracy calculated with all these indices, along with their corresponding contribution explanations by the SHAP tree explainer.

For precipitation-related extreme climate indices (Fig. 2a) the CT showed the best performance ($R^2 = 0.15$, RMSE = 0.084) in forecasting end-of-growing season GPP followed by R95p ($R^2 = 0.14$, RMSE = 0.114), Rx1day index ($R^2 = 0.11$, RMSE = 0.115), CWD ($R^2 = 0.09$, RMSE = 0.119) and Rx5day ($R^2 = 0.04$, RMSE = 0.122) in the early season (MJ). As the seasons progressed and information from the previous season was incorporated into the LightGBM, the accuracy of the model no longer improved. In addition, Rx1day and R95p performed better than other precipitation-related extreme indices in terms of forecasting skills in most growing periods (see Fig. 2a). With respect to the temperature-related extreme indices (Fig. 2b), the TXx index ($R^2 = 0.17$, RMSE = 0.107) performed best in predicting end-of-growing season GPP, followed by the TNx index ($R^2 = 0.13$, RMSE = 0.111). The TXx index showed improved performance when using observations from the early-to-mid growing season (May-July). As the seasons progressed further (e.g., in the full season) the model showed an apparent decreasing skill in forecasting end-of-growing season GPP. The response of end-of-growing season GPP to extreme climate indices was further verified by Pearson correlation analysis (see Fig. S5, S6).

Table 3
Summary of the meteorological, agricultural, and hybrid drought indices.

Drought indices		Input data	References
Category	Abbreviation		
Agriculture drought indices	SMI	Root zone SM product SoMo.ml-EU (0–50 cm)	O et al. (2022)
	SMA	Surface SM product GSSM1km (0–5 cm)	Han et al. (2023)
	SWDI	FC, WP, and SoMo.ml-EU (0–50 cm) content	Martínez Fernandez ét al. (2015)
Hybrid drought index	CDI	FC, WP, SoMo.ml-EU (0–50 cm) content, precipitation, and PET	Chatterjee et al. (2022)
Meteorological drought indices	SPI	Precipitation	McKee et al. (1993)
	SPEI	Precipitation, PET	Vicente Serrano et al. (2010)

Note: SMI - Root Zone Soil Moisture-based Index; SMA - Surface Soil Moisture Index; SWDI - Soil Water Deficit Index; CDI - Comprehensive Drought Index; SPI - Standardized Precipitation Index; SPEI - Standardized Precipitation Evapotranspiration Index; SM - Soil Moisture.

Based on the model's forecast accuracy (see Fig. 2a) using individual indices as predictors Rx1day has a higher impact on GPP, whereas the cumulative precipitations Rx5day and CT have relatively low R^2. The instant maximum precipitation within a 16-day period is more influential on plant growth than other precipitation-related indices. This implies that the duration of precipitation may hardly stimulate plant growth compared with instant maximum precipitation within 16 days. The prediction of plant growth also appears to be more sensitive to extreme absolute temperature measures (TXx and TNx) than to relative ones (TX90p and TN90p).

For individual drought indices (Fig. 2c) it is seen that as more data from the previous season were included in the LightGBM model for predicting end-of-growing season GPP the accuracy increased from the early season to the full growing season. The improved performance suggests that including late-season data appears to improve the accuracy of GPP estimations. In general, the agriculture and hybrid drought indices (i.e., SMI, SMA, SWDI, CDI) performed better than the meteorological drought indices (i.e., SPI, SPEI). The meteorological drought indices, SPEI outperformed SPI in all seasons, indicating the importance of evapotranspiration in plant growth. For the agricultural and hybrid drought indices the order of decreasing performance for early season forecasts (May–June) is as follows: SMA > SWDI > SMI > CDI. For early-to-mid (May-July and May-August) and full-seasons (May-September and May-October) the CDI outperformed other drought indices, followed by SWDI, SMA, and SMI. Overall, SMA dominated early-season forecasts; however, the CDI dominated early-to-mid and full-season forecasts.

Table 4 shows the combinations of all extreme climate indices and drought indices used for forecasting end-of-growing season GPP in different growing seasons. The result indicates that the forecasting accuracy of LightGBM model increases from the early season (R^2=0.35,

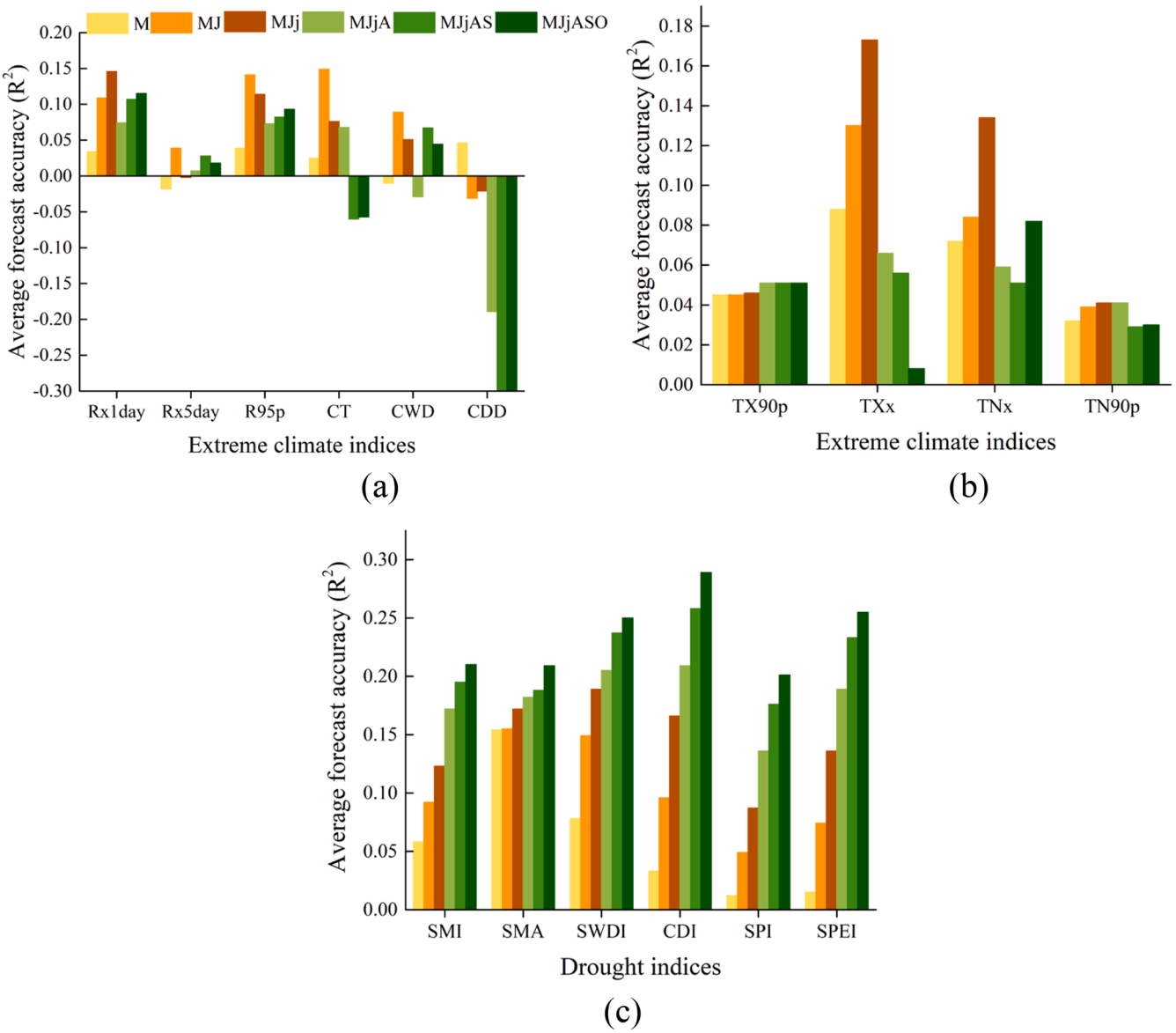

Fig. 2. LightGBM model performance. Performances of (a) precipitation-related extreme climate indices, (b) temperature-related extreme climate indices, and (c) drought indices for different growing periods in predicting end-of-growing season GPP in Europe on test datasets. Note: The y-axis represents the LightGBM model's prediction R^2 on test datasets. Growing periods M = May; MJ = May-June; MJj = May-June-July; MJjA = May-June-July-August; MJjAS = May-June-July-August-September; and MJjASO = May-June-July-August-September-October.

Table 4
Prediction results at different growing periods in predicting end-of-growing season GPP incorporating all extreme climate predictors with the LightGBM model.

Growing periods	LightGBM	
	R^2	RMSE (kg C/m^2)
M	0.35	0.148
MJ	0.38	0.141
MJj	0.43	0.134
MJjA	0.43	0.133
MJjAS	0.44	0.133
MJjASO	0.45	0.136
Average	0.41	0.138

Note: For the abbreviation of growing periods, refer to Fig. 2.

RMSE=0.418) to the full season (R^2=0.45, RMSE=0.136). In summary, the combination of multiple indices increased model prediction.

The importance of all extreme climate events, as described by 16 indices (see Fig. 1), in predicting end-of-growing season GPP is determined using the SHAP algorithm (Fig. 3). Fig. 3 displays the summary plots of six sub-LightGBM forecast models corresponding to different growing periods, with each model explained using the SHAP algorithm. The y-axis in Fig. 3 represents the relative importance of predictors to the model predictions. Here, each predictor derived from two dates within a month, specifically, the first 16 days (i.e., M1, J1, j1, A1, S1, O1) and the latter 16 days of the month (i.e., M2, J2, j2, A2, S2). For each sub-model, the summary plot shows the eight most important predictors.

The SPEI, SMI, and Rx1day played a less significant role than SMA, TNx, and TXx in May (Fig. 3a). In the early and early-to-mid season the SMA, TXx, TNx, and SPEI improved the model accuracy (Fig.3a-3d). For the full season (i.e., May-September and May-October) the SMA, TXx, and TNx played a dominant role (Fig. 3e and 3f).

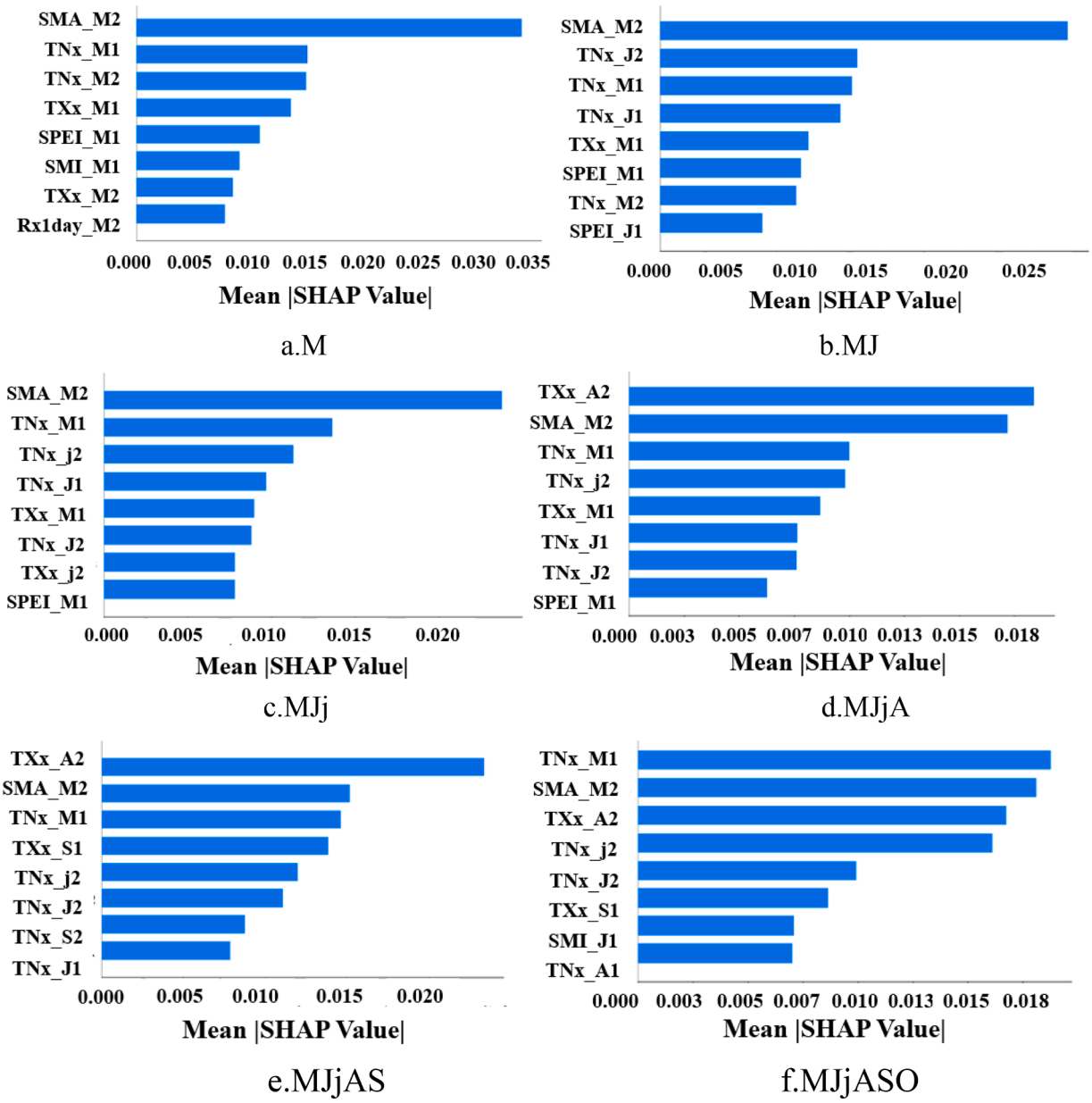

Fig. 3. SHAP summary plots. The plots illustrate the importance of predictors in different periods of the growing seasons in predicting end-of-growing season GPP. Note: The x-axis denotes the average impact on the model output. The y-axis represents important predictors, with the predictor indicated before the hyphen and the corresponding month denoted after the hyphen. The numbers 1 and 2 (M1 and M2) signify the first 16 days and the latter 16 days within a month. The growing period abbreviations (M, MJ, MJj, MJjA, MJjAS, and MJjASO) are defined in Fig. 2.

In summary, surface soil moisture-related agricultural drought (SMA) and extreme absolute temperature (i.e., TNx and TXx) are the dominant factors with respect to plant growth in all the growing periods. The other indices' contribution diverges dramatically in forecasting end-of-growing season GPP at different growing periods. It should be noted that the occurrence of agricultural drought in the second half of May, as indicated by SMA_M2 (refer to subfigures a-f), is identified as a significant predictor for the end-of-growing season GPP prediction during all growing seasons. This suggests the potential existence of drought memory.

3.2. Forecast skill across climate regimes

The model's forecast performance for end-of-growing season GPP is evaluated separately in arid, temperate, and cold climate regimes (see Supplementary Fig.S2 for climate regimes division) to identify the

Table 5
LightGBM model performances at different growing periods in predicting end-of-growing season GPP across three climate regimes.

Growing periods	Cold climate regime		Arid climate regime		Temperate climate regime	
	R^2	RMSE (kg C/m^2)	R^2	RMSE (kg C/m^2)	R^2	RMSE (kg C/m^2)
M	0.42	0.137	0.45	0.094	0.28	0.150
MJ	0.44	0.132	0.51	0.087	0.29	0.145
MJj	0.45	0.130	0.58	0.077	0.29	0.138
MJjA	0.45	0.130	0.60	0.072	0.28	0.134
MJjAS	0.46	0.131	0.60	0.073	0.28	0.131
MJjASO	0.47	0.135	0.61	0.074	0.29	0.131
Average	0.45	0.133	0.56	0.080	0.29	0.138

Note: The abbreviation of growing periods refers to Fig. 2.

dominant predictors driving plant growth across three climatic zones. The prediction accuracy decreases in the following order from arid climate (average R^2=0.56, RMSE=0.080) > cold climate (R^2=0.45, RMSE=0.133) > temperate climate (R^2=0.29, RMSE=0.138) (see Table 5). Extreme climate events exert a more direct and significant impact on plant growth in arid and cold regions, leading to a stronger correlation with GPP. However, in temperate climates the complexity of ecosystems may introduce other ecological drivers, thereby reducing the apparent correlation between extreme climate events with GPP. The forecasting accuracy increased from the early to full season in arid and

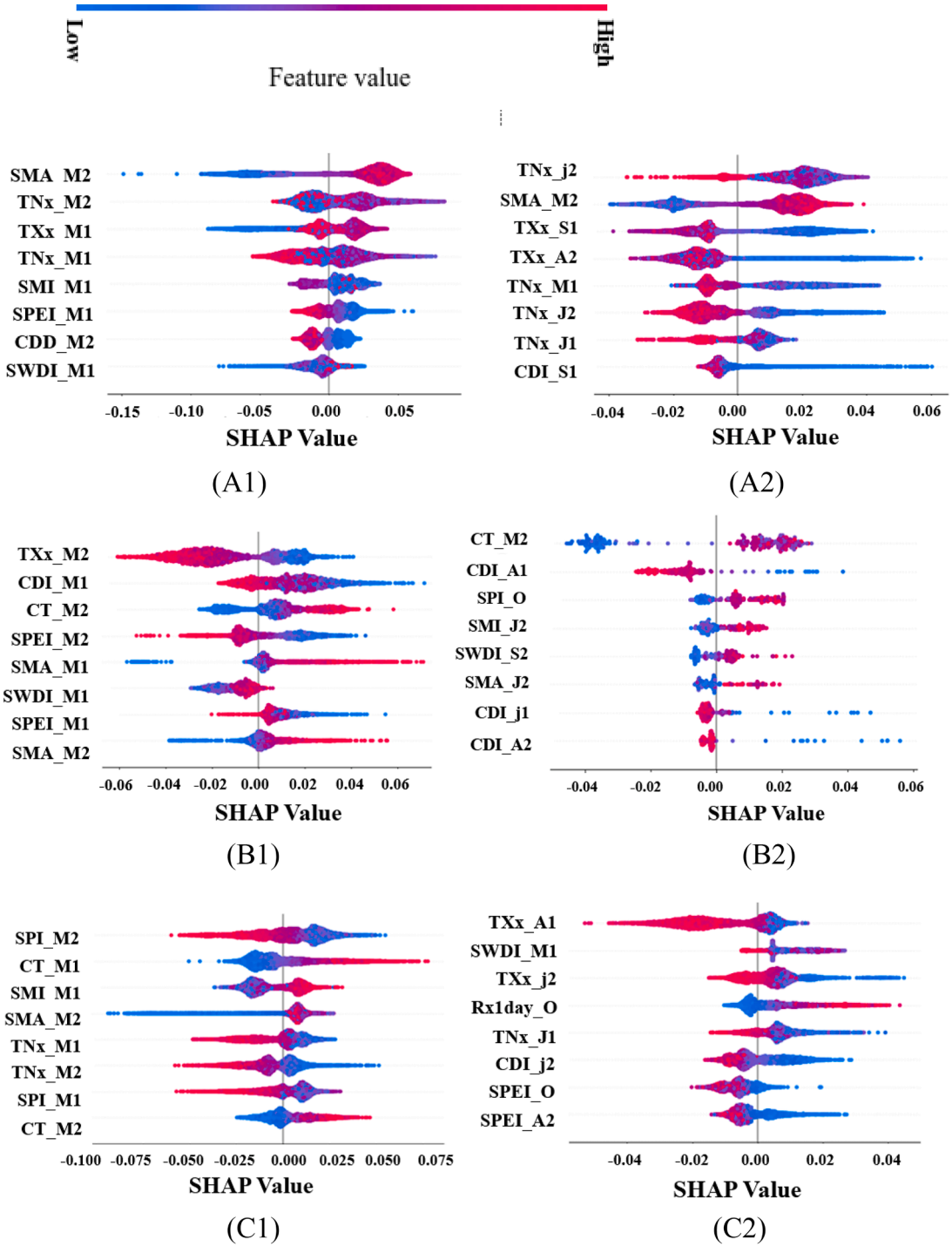

Fig. 4. Beeswarm summary plots illustrating the predictor importance across (A) cold, (B) arid, and (C) temperate climate regimes on test datasets. The LightGBM performance for predicting the end-of-growing season GPP is shown only for the early M (1), and full growing seasons MJjASO (2). Model forecasts for other growing periods are shown in Supplementary Fig. S9. Beeswarm summary plots provide an information-dense summary of how the predictors influence the model's output. The marginal contribution of each predictor to this prediction is demonstrated by their rank from top to bottom. Each instance of the given explanation is represented by a single dot on each predictor row. The color indicates the predictor value itself (red corresponds to high values, and blue corresponds to low values). A negative SHAP value indicates a decrease in the corresponding predictor, which increases the GPP prediction value. Conversely, a positive SHAP value represents a decrease in the corresponding predictor, leading to a decline in the GPP prediction value. The horizontal position of each point represents the SHAP value for the corresponding predictor. For the abbreviation of growing periods, refer to Fig. 2.

cold climates. However, there was no significant improvement in the forecasting skill in temperate climates.

The positive or negative effect of extreme climate events on GPP prediction across different climate regimes is evaluated using the SHAP algorithm (Fig. 4). In cold climates, SMA, TNx, and TXx are important in the early season, closely followed by SMI and SPEI (Fig. 4A1). However, the contributions of SMI and SPEI to the prediction results are not significant in the full season (Fig. 4A2). The same phenomenon is also observed in the early-to-mid season (Fig.S9A3, A4). The SMA values show high feature values in most samples corresponding to positive SHAP values (see Fig. 4, red color). Hence, an increase in topsoil moisture leads to an increase in the end-of-growing season GPP values. Fig. 4 indicates that higher temperatures have less of a negative effect or even a positive impact on GPP in the early growing season. In some cases, TXx and TNx for M1 and M2 show a positive correlation with GPP (i.e., high temperatures lead to an increase in GPP), as shown in Supplementary Fig. S9 A4, TNx_M2. In contrast, high temperature values for the mid-growing season (JjA) tend to be more clearly associated with negative SHAP values (Fig. S9 A4, TXx_A2), displaying a negative correlation with GPP.

In arid climate regimes (Fig. 4B) the model predictors exhibit significant variations compared to those in cold climate regimes (Fig. 4A). CDI, CT, and TXx are important in the early (see Fig. 4B1). This pattern is also displayed in early-to-mid growing seasons (see Fig.S9B3, B4). In the early season CDI, CT, and TXx are prominent predictors, followed by SPEI. In the full season (Fig. 4B2), the significance of SWDI for forecasting end-of-growing season GPP becomes pronounced, playing a more prominent role compared to earlier months. Fig. 4B2 showed the occurrence of meteorological drought with low SPI values, represented by a blue color, corresponding to negative SHAP values. Hence, severe meteorological droughts given by low SPI values decrease the predicted GPP values.

For the temperate climate regime, meteorological drought indices (SPI) and CT are identified as important predictors by the LightGBM model in the early season in predicting GPP (Fig. 4C1). The low CT value with blue color corresponds to negative SHAP values, indicating that a decrease in maximum consecutive precipitation amounts tends to increase the end-of-growing season GPP. In the full-growing seasons (Fig.4C2), TXx, SWDI, and CDI are the main driving predictors. A similar trend is observed in the early-to-mid growing season (Fig. S9C3, C4).

Overall, the dominant indices diverge dramatically, largely depending on the climate regime and growth stage of forecast (i.e., early, early-to-mid, and full season). Please note that extreme absolute temperatures (TNx/TXx) play a significant role in all climates. In cold climates, agricultural drought indicated by surface soil moisture (SMA) dominates the model's precipitation performance for the end-of-growing season GPP. In arid climates, hybrid meteorological and agricultural drought indicated by CDI and maximum consecutive n-days total precipitation amount (CT) outperforms other indices, except for TXx, across all growth stages. In temperate climates TNx remains the dominant factor during all the growing seasons, with the CDI closely following behind. Nevertheless, the predictors exhibit complex relationships across different growth stages in temperate climates, in contrast to the relatively consistent patterns observed in cold and arid climates.

3.3. Forecast skill in agricultural landcover types

There are six broad LC types (see Supplementary Fig. S3a). This study specifically investigates how extreme events affect the agricultural LC types (grassland, irrigated, and rain-fed cropland) focusing on the end-of-growing season GPP (see Appendix Fig. S3b). The model forecasting performances over irrigated and rainfed croplands, and in grasslands, are presented in Table 6.

The model performed best for rainfed croplands (R^2=0.51, RMSE=0.070), followed by grasslands (R^2=0.41, RMSE=0.139), and irrigated croplands (R^2=0.34, RMSE=0.093). For all land use classes, the results are best when using predictors from the early season. The addition of further predictors from later months did not improve the model's performance.

Table 6
LightGBM model performances at different time steps in predicting end-of-growing season GPP across agricultural landcover types.

Growing periods	Irrigated croplands		rainfed croplands		Grasslands	
	R^2	RMSE	R^2	RMSE	R^2	RMSE
M	0.36	0.095	0.52	0.074	0.43	0.138
MJ	0.36	0.094	0.53	0.069	0.44	0.137
MJj	0.36	0.089	0.53	0.068	0.43	0.137
MJjA	0.33	0.091	0.50	0.069	0.39	0.140
MJjAS	0.31	0.093	0.49	0.071	0.39	0.140
MJjASO	0.30	0.095	0.51	0.070	0.38	0.144
Average	0.34	0.093	0.51	0.070	0.41	0.139

Note: The abbreviation of growing periods refers to Fig. 2.

The Sankey diagram (Fig. 5A–C) is derived from summary plots of the SHAP algorithm which delineates the intricate relationships between extreme climate events and the different growing seasons. Details concerning this matter are presented in Supplementary Fig. S10. The left column represents climate indices, while the right column denotes distinct growing periods of plant growth. The flows in the diagram illustrate the contribution of various extreme climate events during each growth period, with the thickness of the flow lines indicating the degree of importance. Thicker lines signify greater importance on plant growth.

For irrigated croplands SMA, TNx, and TXx are consistently identified as three important predictors in forecasting the end-of-growing season GPP throughout the entire growing period (see Fig. 5A). In the early-to-mid growing season, SWDI is also recognized as an important predictor for forecasting plant growth (Fig. S10A3, A4), in addition to the three previously cited key factors. Notably, for the full season, CDI makes a significant contribution, alongside the three significant predictors, as explained by the SHAP algorithm (see Fig. S10A5, A6). In rainfed croplands, SMA, TXx/TNx, and SWDI outperformed other indices in all growing season forecasts (Fig. 5B). SMA, TNx/ TXx, and SMI played dominant roles in forecasting plant growth in grasslands in all seasons, including SPEI in the early season (Fig. 5C). The SPEI and SMI played crucial roles, closely following SMA in the full growing seasons.

To further explore how leading predictors including SMA, TXx, TNx, SWDI, and SMI change the model's output, this work applied a dependence plot of the SHAP algorithm to show the relationships between individual predictors and prediction end-of-growing season GPP. Specifically, Fig. 6 displays the dependence plots for rainfed croplands in May as an example. The dependence plots for agricultural lands (i.e., rainfed, irrigated croplands, and grasslands) across different growing seasons (i.e., M, A, O), which represent early-stage, mid-stage, and late-stage, respectively, can be found in the supplementary Fig. S11. Fig. 6 reveals that the rising values of SMA increase SHAP Value. When the SMA value is larger than 0.23, the SHAP values are positive (above the gray dashed line), indicating a positive correlation with the model's prediction of the end-of-growing season GPP. It suggests that the increase in SMA leads to an increase in the end-of-growing season GPP. The same applies to the SMI dependence plot when the SMI value is larger than 0.25, the SHAP values exceed zero. However, SHAP value decreases with increasing TXx value. When TXx exceeds 31 °C, the corresponding SHAP value is consistently less than 0. It indicates that the increase in TXx results in a decrease in the end-of-growing season GPP. The same trend is observed with TNx: when TNx is greater than 14 °C the corresponding SHAP value is less than zero. Specifically, exceeding the maximum temperature or the maximum of all daily minimum temperatures within a 16-day window leads to a reduction in GPP. Here, the predictor value corresponding to a SHAP value of 0 is considered as the threshold. SWDI, calculated based on soil hydraulic

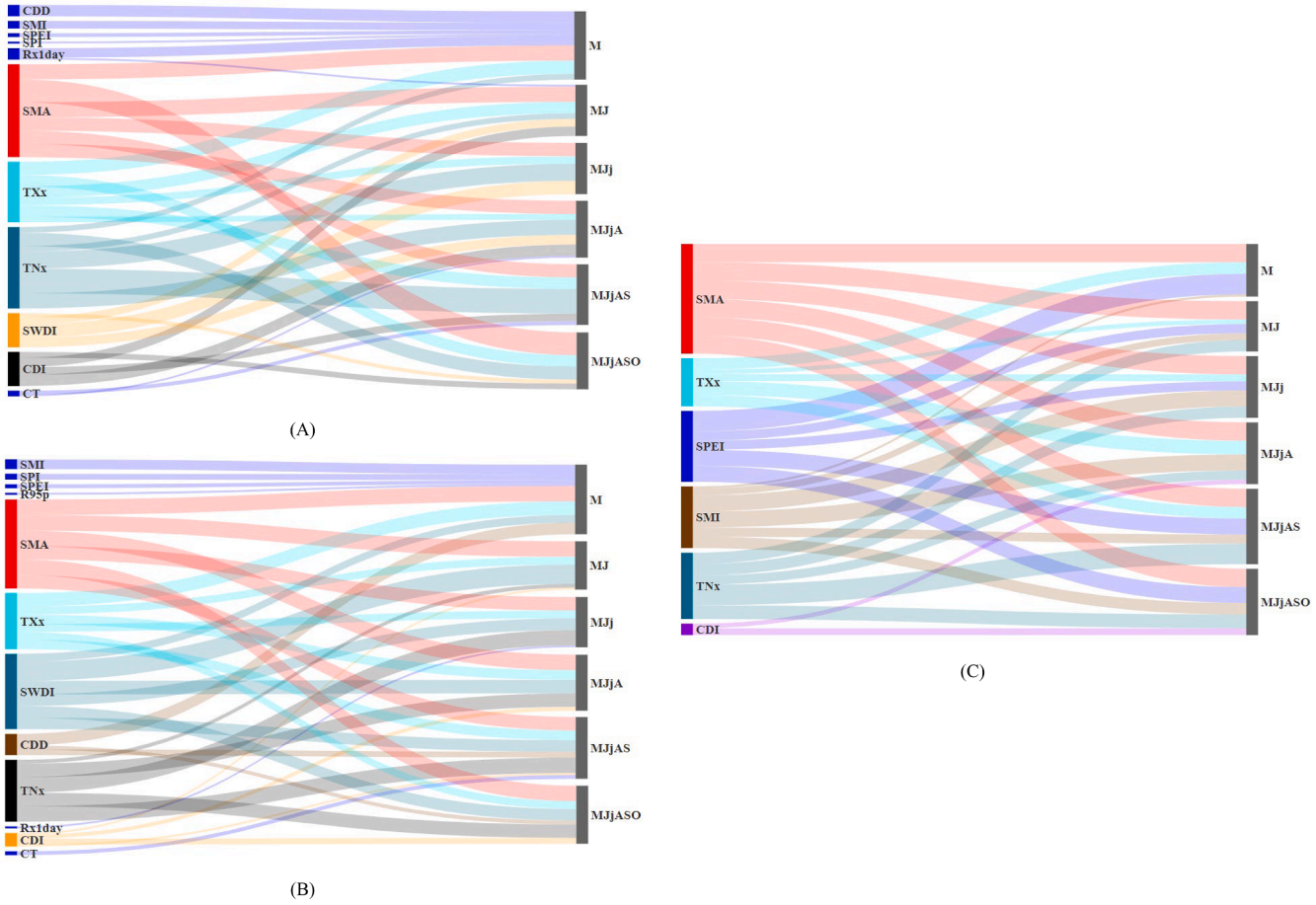

Fig. 5. Sankey diagram illustrating the variable importance across (A) irrigated croplands, (B) rainfed croplands, and (C) grasslands at different growing periods: (1) M, (2) MJ, (3) MJj, (4) MJjA, (5) MJjAS, and (6) MJjASO, using LightGBM for end-of-growing season GPP forecasting. The abbreviations for the growing periods are presented in Fig. 2.

properties, was scaled to a range of 0–1, where 0 indicates dry soil, close to the wilting point, and 1 indicates wet soil, close to the field capacity (see Supplementary Equation 2). SHAP values increase with higher SWDI values, becoming positive above a SWDI value of 0.015. The increase in SWDI leads to an increase in GPP. Thus, the tipping points where positive and negative SHAP values contribute to a shift in the end-of-growing season GPP are around 0.23 (SMA), 0.25 (SMI), 31 °C (TXx), 14 °C (TNx), and 0.015 (SWDI).

It is noteworthy that there is not just one tipping point. Furthermore, the selection of the growing season period used for the indicator in defining tipping points is important. Specifically, there are two tipping points in the dependence plot for TNx in late August and October (see Supplementary Fig. S11 a9,a14), for TXx in October (see Fig. S11a13, b13), and for SMA in October (Fig.S11a11,b11). This means that there is an increased or decreased effect on end-of-growing season GPP between those two tipping points, while outside of those points, the effect changes in the opposite direction. Moreover, the high-temperature extreme value either increases or decreases end-of-growing season GPP depending on the growing periods (Fig. S11 a1 VS a11; b9 VS b14) and landcover types (Fig. S11 a11 VS c11). Similar patterns were also observed for soil moisture (see Fig. S11 a11, b11).

4. Discussion

4.1. Timing of extreme events may impact the end-of-growing season GPP differently

This study used extreme climate events during different periods of growing seasons to forecast end-of-growing season GPP, identifying their contribution to the output of the explainable LightGBM model. Our findings suggest that extreme events in the early season primarily control GPP, even the strength of the impact depends on the climate regime. In general, the occurrence of agricultural droughts in the early growing season has positive effects on the end-of-growing season GPP, suggesting the potential existence of drought memory (see Fig. 3). The timing of extreme climate events within different growing seasons has either positive or negative effects on end-of-growing season GPP forecast. Specifically, a high temperature extreme event in the early growing season may have a positive effect, while it might have a more pronounced negative effect in the later growing season. Similar patterns for soil moisture, with some differences observed across climate regimes, as shown in Fig. 4. In cold climate regions, the occurrence of agricultural drought (SMA) in the early growing season and extreme absolute temperatures (TXx and TNx) in full growing seasons influence model forecast performance. These effects are positive and negative, respectively. For arid climates, hybrid drought, extreme high temperature, and consecutive precipitation events in early and early-to-mid growing seasons play a dominant role in model performance. The role of SWDI in forecasting end-of-growing season GPP becomes pronounced in the late growing season, with a positive impact. In temperate climate regions, meteorological drought and consecutive precipitation events occurring early in the season are important for model results. It should be noted that for SPEI, the impact may be negative when it occurs in the early season and positive in the mid and late seasons. The possible reason is that plants adjust and cope with drought effects over time (Osakabe et al., 2014; Seleiman, et al., 2021). Meteorological drought can exert

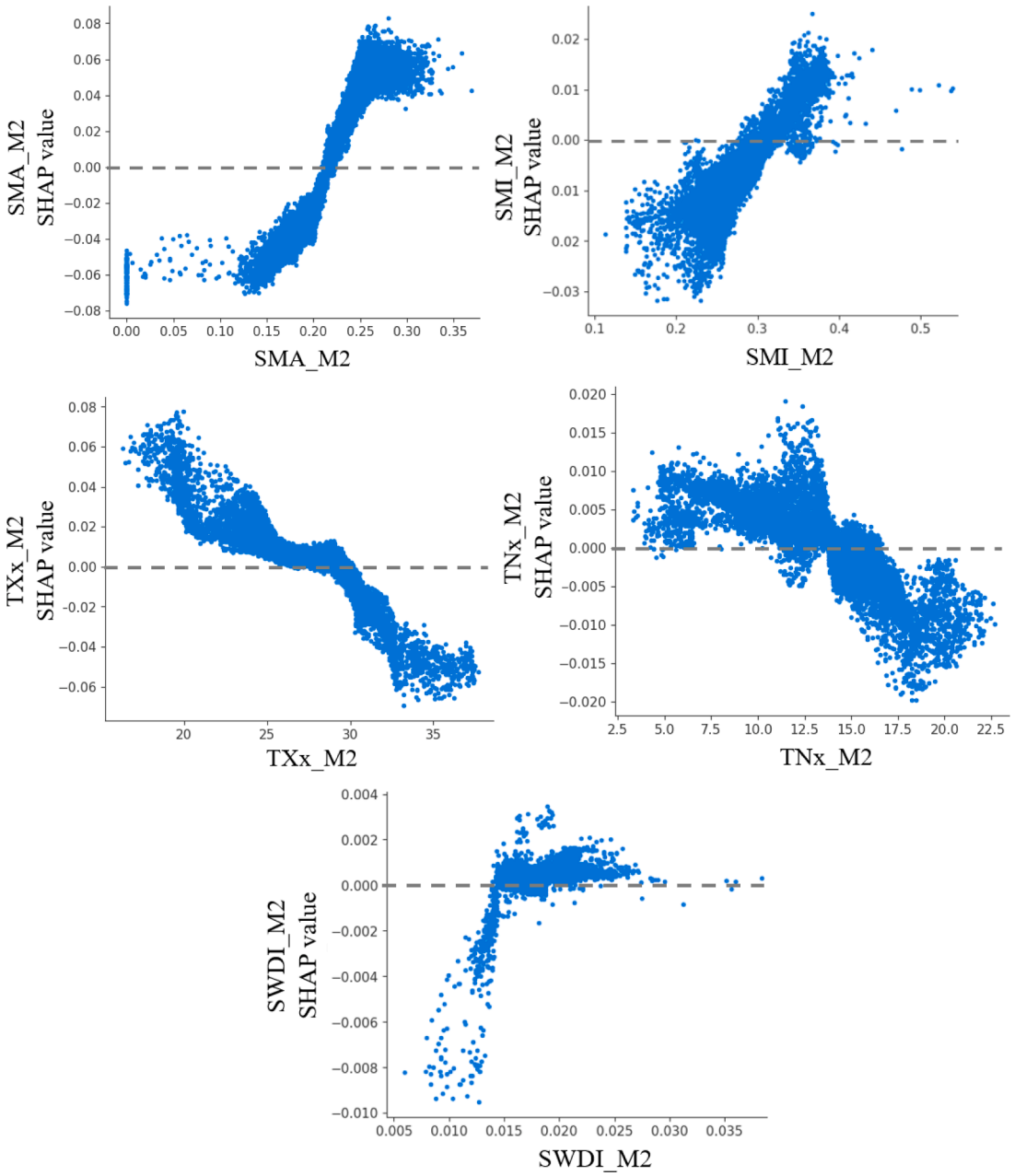

Fig. 6. Dependence plots illustrating the relationship between individual variables and model output across agricultural croplands (using Rainfed Croplands in the early growing seasons as an example) with LightGBM for end-of-growing season GPP forecasting. The gray dashed line represents SHAP values equal to zero. The x-axis represents the values of a selected predictor, while the y-axis shows the corresponding SHAP value which quantifies the contribution of each feature to the model predictions. SHAP value greater than 0 indicates a positive influence of the feature on the model's prediction of the end-of-growing season GPP.

stress on plants due to both limited water supply and high evaporation, leading to a negative impact on GPP (Pascolini-Campbell, 2022). In contrast, during the mid and late growing season, when plants are more mature and less dependent on water, moderate drought may promote maturity and improve yield, resulting in a positive impact on GPP (Hahn et al.,2021). Extreme high temperatures, hybrid droughts occurring in the early-to-mid growing season, and soil water drought events in the early growing season have negative effects on end-of-growing season GPP forecasts. The effective prevention of specific extreme climate events and focus on their effects in different periods of growing seasons may largely improve yield.

4.2. Dominant extreme climate events across different climate regions

Extreme absolute temperatures (TNx/TXx) exert a more substantial impact on plant growth across all climates. Extreme absolute temperatures (TXx and TNx) directly affect plant physiological processes. High temperatures elevate evapotranspiration, while low temperatures can cause freezing and damage to plant cell structures (Hatfield and Prueger, 2015). These physiological effects impact plant productivity and development. Extreme temperatures also impact soil moisture availability. High temperatures increase soil moisture evaporation, diminishing water availability for plants. In summary, extreme absolute temperatures play a vital role in shaping the conditions for plant growth across various climates and agricultural environments. Plant growth sensitivity to extreme climate events is higher in cold and arid climates

compared to temperate climates. In cold climates, the primary factor is agricultural drought indicated by surface soil moisture (SMA), while in arid climates, the leading factor is the duration of extreme precipitation induced by the maximum consecutive n-days precipitation amount (CT). Water scarcity is the principal limitation of plant growth in arid climates. An increase in continuous maximum rainfall days may enhance soil water storage, positively impacting vegetation growth. However, in cold regions, soil moisture is influenced by various factors such as snowmelt and rainfall infiltration (Fu et al., 2018). Therefore, topsoil moisture directly reflects available moisture conditions.

4.3. The differential performance of extreme climate events on agricultural land considering various irrigation methods

The LightGBM model demonstrates superior forecasting performance in grasslands and rainfed croplands compared to irrigated croplands. Rainfed croplands, unlike irrigated ones, are more vulnerable to the impact of extreme climate events. This study underscores that irrigation can mitigate the impact of climate extremes on plant growth, aligning with findings from Thiery et al. (2017) and Xia et al. (2021). Previous studies have shown that in major agricultural regions, such as the US High Plains, California's Central Valley, and the Indo-Gangetic Basin, irrigation-induced cooling can limit the maximum growing season temperatures, alleviate heat extremes, and counteracts anthropogenic warming trends (McDermid et al., 2021). Additionally, irrigation may affect both local moisture recycling and remote precipitation patterns through interactions with larger-scale atmospheric circulation (Yang et al., 2023).

In the agricultural LC types soil moisture-related agriculture drought (i.e., SMI, SMA, and SWDI) exhibits a stronger correlation with GPP compared to hybrid (i.e., CDI) and meteorological drought (i.e., SPI and SPEI) (see Supplementary Fig. S7). This is so because soil water dynamics are governed by nonlinear interactions among different hydrometeorological and biophysical processes controlling precipitation, evapotranspiration, and runoff (Ghannam et al., 2016). These interactions make soil moisture a key regulator of plant growth and nutrient uptake (Grillakis, 2019). The robust correlations between GPP and soil moisture drought indices are also evident in the coterminous United States (CONUS, Chatterjee et al., 2022). Thus, soil moisture can be used as a key indicator to assess global plant growth and crop yields.

The LightGBM model exhibited superior forecast performance for the surface soil moisture (SMA) compared to the root zone soil moisture (SMI) in agricultural land types. The differing roles of the two soil moisture indices in forecasting end-of-growing season GPP may be attributed to soil moisture anomalies typically emerging first in the topsoil layer and later extending to the entire soil layer (Tijdeman and Menzel, 2021; Pinke et al., 2022). The increased frequency of heavy rainfall events in Europe, coupled with a higher proportion of surface runoff and reduced infiltration (IPCC, 2019), results in a decreased amount of water penetrating the soil. While this reduced water can partially compensate for soil moisture deficits in the top layers, it may struggle to replenish moisture levels in the deeper layers.

4.4. Data quality and model uncertainties across climate regions and agricultural land cover types: insights from selected indicators

Data quality may have influenced the results presented in this work, including the quality of soil moisture and extreme climate indices. Inaccurate soil moisture data could introduce errors into our model forecasts, potentially skewing our understanding of its impact on GPP. This study's results reveal that the highest positive correlation between soil moisture drought indices and GPP is observed in southern and southwestern Europe (see Appendix Fig. S8). In contrast, the largest negative correlation is found in northern European regions, likely due to a lack of available soil moisture data related to low surface temperatures, as noted in the supplementary Information (see Fig. S8). Denissen et al. (2020) also report low soil moisture data quality in Northern Europe, where the climate regime is predominantly cold, and grassland predominate. This study has shown that the error introduced by soil moisture primarily influences model performance in cold climate regimes. For agricultural land covers the model's performance may also be affected (see Fig. S3). However, we are confident that our large-scale analysis is robust and yields meaningful results despite data uncertainties. Furthermore, a root zone soil moisture depth of 50 cm was utilized in this study, which is relatively shallow for fully representing root zone soil moisture (Li et al., 2023). In addition, the calculation of consecutive indices (Rx5days, CT, CWD, CDD) within a 16-day window may underestimate the magnitude of an extreme event, especially if the event occurs mid-month, exactly during the interface between two 16-day periods. These issues represent potential avenues for future research.

4.5. Prospects

This study was built upon the methodology of Chatterjee et al. (2022) to focus on the impact of extreme climate events on plant growth and to identify tipping points in Europe. Future work shall use high-quality soil moisture products, especially in northern Europe, as these data become available, to improve data quality and enhance the robustness of the analysis. In addition, root zone soil moisture products with deeper soil layers shall be used to evaluate our forecasts. This would reduce the uncertainty of root zone soil moisture products. This study focuses on the period from May to mid-October to avoid frozen soil conditions which may not well reflect biomass and yield production for winter crops. Therefore, the impact of extreme climate events on the yields of specific crops will be explored, especially with respect to winter crops, in future studies. However, indices for larger time scales (e.g., 30-days) could be used to dismiss the impact of the magnitude of an extreme event, especially if the event occurs mid-month during the interface between two 16-day periods. Although this study did not conduct a causality analysis using a lagged time series of extreme climate events with GPP, it is acknowledged that this is a potential avenue for future research. Additionally, the climatological definition of extreme climate events has inherent limitations. It is suggested that a synthetic definition be employed to represent "extreme climate events" concerning driving and response variables, with a specific emphasis on how climatic conditions influence plant mortality and impede plant growth.

The findings of this study contribute to understanding how plant growth responds to extreme climate events, consistent with prior research suggesting the critical importance of such events for plant growth and their potential utility in crop yield estimation (Sun et al., 2021). These advancements will enhance our methodology for predicting the impact of extreme climate events on GPP, thereby strengthening its applicability as a valuable tool for agricultural adaptation management.

5. Conclusions

This study assessed the response of the end-of-growing season GPP to extreme climate events. Specifically, it investigated the predictive capability of ten temperature and precipitation-related extreme climate indices, along with six meteorological, agricultural, and hybrid drought indices, on plant production (using GPP as a proxy) employing an ML (LightGBM) model across various climate regimes, agricultural land types, and irrigation practices in Europe. The explainable LightGBM model was applied to analyze the impact of various weather extremes occurring in different periods of the growing season (early, early-to-mid, and full) on the end-of-growing season GPP. The key insights and conclusions of this study are as follows:

The growth of plants is influenced by the intricate interplay of various extreme climate events, which vary across climate regimes,

landcover types, and growing seasons. The SHAP approach was applied in this work to identify key extreme climate events, their timing effects, and tipping points during plant growth. Notably, drought memory, especially early-season soil moisture controls the early stages of plant growth with some differences across climate regimes. Extreme climate events in different growing seasons have either positive or negative effects on the end-of-growing season GPP forecast, largely depending on their timing. There is more than one tipping point. The selection of the specific month or time period used for the indicator in defining tipping points is quite important. Moreover, among the three agricultural landcover types the poorer prediction results in irrigated croplands suggest that the implementation of irrigation strategies involving human intervention would help mitigate the impact of extreme climate events. Overall, properly accounting for the above mentioned factors can further improve crop yield estimation. Our methodology is well-suited for continental and multidecadal forecasts, making it a valuable tool for managing agricultural adaptation.

Funding

This work was supported by the Einstein Research Unit "Climate and Water under Change" from the Einstein Foundation Berlin and Berlin University Alliance (ERU-2020–609).

CRediT authorship contribution statement

Huihui Zhang: Writing – review & editing, Writing – original draft, Visualization, Validation, Software, Methodology, Formal analysis, Data curation, Conceptualization. **Hugo A Loaiciga:** Writing – review & editing, Validation, Supervision. **Akpona Okujeni:** Writing – review & editing, Conceptualization. **Ji Liu:** Writing – review & editing, Visualization. **Min Tan:** Writing – review & editing. **Tobias Sauter:** Writing – review & editing, Supervision, Project administration, Funding acquisition.

Declaration of competing interest

The authors declare that they have no known competing financial interests or personal relationships that could have appeared to influence the work reported in this paper.

Acknowledgments

We acknowledge the E-OBS dataset and the data providers in the ECA&D project (https://www.ecad.eu).

Supplementary materials

Supplementary material associated with this article can be found, in the online version, at doi:10.1016/j.agrformet.2024.110374.

Data availability

The data and code for this research work are available from 10.6084/m9.figshare.25406971. Their access approaches are displayed in Supplementary data.

References

Abdollahi, A., Pradhan, B., 2023. Explainable artificial intelligence (XAI) for interpreting the contributing factors feed into the wildfire susceptibility prediction model. Sci. Total Environ. 879, 163004.
Anderson, T.W., Sclove, S.L., 1978. An Introduction to the Statistical Analysis of Data. Houghton Mifflin Company, Boston.
Beck, H.E., et al., 2018. Present and future Köppen-Geiger climate classification maps at 1-km resolution. Sci. Data 5 (1), 1–12.
Chatterjee, S., et al., 2022. Soil moisture as an essential component for delineating and forecasting agricultural rather than meteorological drought. Remote Sens. Environ. 269, 112833.
Chen, J., et al., 2023. Divergent response of crops and natural vegetation to the record-breaking extreme precipitation event in 2020 modulated by topography. Environ. Res. Lett.
Cheng, M., et al., 2023. A new drought monitoring index on the Tibetan Plateau based on multisource data and machine learning methods. Remote. Sens. 15 (2), 512.
Chiang, F., Mazdiyasni, O., AghaKouchak, A., 2021. Evidence of anthropogenic impacts on global drought frequency, duration, and intensity. Nat. Commun. 12 (1), 2754.
Christoph, M., 2019. Interpretable Machine learning: A guide For Making Black Box Models Explainable. Lulu. com.
Ciais, P., et al., 2005. Europe-wide reduction in primary productivity caused by the heat and drought in 2003. Nature 437 (7058), 529–533.
Cornes, R.C., et al., 2018. An ensemble version of the E-OBS temperature and precipitation data sets. J. Geophys. Res.: Atmos. 123 (17), 9391–9409.
Dai, A., Zhao, T., Chen, J., 2018. Climate change and drought: a precipitation and evaporation perspective. Current Climate Change Reports 4, 301–312.
Denissen, J.M., et al., 2020. Critical soil moisture derived from satellite observations over Europe. J. Geophys. Res.: Atmos. 125 (6), e2019JD031672.
Dikshit, A., Pradhan, B., Alamri, A.M., 2021. Long lead time drought forecasting using lagged climate variables and a stacked long short-term memory model. Sci. Total Environ. 755, 142638.
Ebi, K.L., Bowen, K., 2016. Extreme events as sources of health vulnerability: Drought as an example. Weather and Clim. Extrem. 11, 95–102.
Feng, L., et al., 2021. Geographically and temporally weighted neural network for winter wheat yield prediction. Remote Sens. Environ. 262, 112514.
Fischer, E.M., et al., 2014. Models agree on forced response pattern of precipitation and temperature extremes. Geophys. Res. Lett. 41 (23), 8554–8562.
Franke, G.R., 2010. Multicollinearity. Wiley international encyclopedia of marketing.
Frich, P.A.L.V., et al., 2002. Observed coherent changes in climatic extremes during the second half of the twentieth century. Climate Res. 19 (3), 193–212.
Friedl, M., Sulla-Menashe, D., 2022. MODIS/Terra+Aqua Land Cover Type Yearly L3 Global 500m SIN Grid V061 [Data Set]. NASA EOSDIS Land Processes Distributed Active Archive Center. https://doi.org/10.5067/MODIS/MCD12Q1.061. Accessed 2023-06-01 from.
Fu, Q., et al., 2018. Effects of soil water and heat relationship under various snow cover during freezing-thawing periods in Songnen Plain. China. Scientific Reports 8 (1), 1325.
Ghannam, K., et al., 2016. Persistence and memory timescales in root-zone soil moisture dynamics. Water Resour. Res. 52 (2), 1427–1445.
Grillakis, M.G., 2019. Increase in severe and extreme soil moisture droughts for Europe under climate change. Sci. Total Environ. 660, 1245–1255.
Gulzar, A.B.M., Mazumder, P.B., 2023. Coping with drought: consequences, responses, and plant growth promoting rhizobacteria mediated amelioration mechanisms in crop plants. Gesunde Pflanzen 1–19.
Hahn, C., et al., 2021. Timing of drought in the growing season and strong legacy effects determine the annual productivity of temperate grasses in a changing climate. Biogeosciences 18 (2), 585–604.
Han, Q., et al., 2023. Global long term daily 1 km surface soil moisture dataset with physics informed machine learning. Sci. Data 10 (1), 101.
Hatfield, J.L., Prueger, J.H., 2015. Temperature extremes: effect on plant growth and development. Weather and Clim. Extrem. 10, 4–10.
Haylock, M.R., et al., 2008. A European daily high-resolution gridded data set of surface temperature and precipitation for 1950–2006. J. Geophys. Res.: Atmos. 113 (D20).
Heim Jr, R.R., 2002. A review of twentieth-century drought indices used in the United States. Bull. Am. Meteorol. Soc. 83 (8), 1149–1166.
Hengl, T., et al., 2017. SoilGrids250m: Global gridded soil information based on machine learning. PLoS One 12 (2), e0169748.
IPCC, 2019. Climate Change and Land: an IPCC special report on climate change, desertification, land degradation, sustainable land management, food security, and greenhouse gas fluxes in terrestrial ecosystems. IPCC.
Iizumi, T., Sakai, T., 2020. The global dataset of historical yields for major crops 1981–2016. Sci Data 7 (1), 97.
Islam, A.R.M.T., et al., 2021. Spatiotemporal nexus between vegetation change and extreme climatic indices and their possible causes of change. J. Environ. Manage. 289, 112505.
Jin, H., et al., 2023. Higher vegetation sensitivity to meteorological drought in autumn than spring across European biomes. Communicat. Earth & Environ. 4 (1), 299.
Khan, N., et al., 2020. Prediction of droughts over Pakistan using machine learning algorithms. Adv. Water Res. 139, 103562.
Krishnamurthy, R, et al., 2022. Anticipating drought-related food security changes. Nature Sustain. 5 (11), 956–964.
Krueger, E.S., Ochsner, T.E., Quiring, S.M., 2019. Development and evaluation of soil moisture-based indices for agricultural drought monitoring. Agron. J. 111 (3), 1392–1406.
Kuśmierek-Tomaszewska, R., Żarski, J., 2021. Assessment of meteorological and agricultural drought occurrence in central Poland in 1961–2020 as an element of the climatic risk to crop production. Agriculture 11 (9), 855.
Li, J., et al., 2022. Regional asymmetry in the response of global vegetation growth to springtime compound climate events. Communic. Earth Environ. 3 (1), 123.
Li, Y., et al., 2019. Excessive rainfall leads to maize yield loss of a comparable magnitude to extreme drought in the United States. Global Change Biol. 25 (7), 2325–2337.
Leng, G., Hall, J., 2019. Crop yield sensitivity of global major agricultural countries to droughts and the projected changes in the future. Sci. Total Environ. 654, 811–821.

Li, M., Sun, H., Zhao, R., 2023. A review of root zone soil moisture estimation methods based on remote sensing. Remote 15 (22), 5361.
Lundberg, S.M., Lee, S.I., 2017. A unified approach to interpreting model predictions. Adv. Neural Inf. Process. Syst. 30.
Ma, J., et al., 2022. MERRA-2 PM2.5 mass concentration reconstruction in China mainland based on LightGBM machine learning. Sci. Total Environ. 827, 154363.
Martínez-Fernández, J., et al., 2015. A soil water based index as a suitable agricultural drought indicator. J. Hydrol. 522, 265–273.
McCormick, E.L., et al., 2021. Widespread woody plant use of water stored in bedrock. Nature 597 (7875), 225–229.
McDermid, S.S., et al., 2021. Minimizing trade-offs for sustainable irrigation. Nat. Geosci. 14 (10), 706–709.
McKee, T.B., Doesken, N.J., Kleist, J., 1993. The relationship of drought frequency and duration to time scales. Proceed. 8th Conf. Appl. Climatol. 17 (22), 179–183.
Molnar, C., 2020. Interpretable Machine Learning. Lulu Press, Morrisville, NC, USA.
Naumann, G., et al., 2021. Increased economic drought impacts in Europe with anthropogenic warming. Nat. Clim. Change 11 (6), 485–491.
Niu, S., et al., 2014. Plant growth and mortality under climatic extremes: an overview. Environ. Exp. Bot. 98, 13–19.
O'Donnell, A.J., et al., 2021. The role of extreme rain events in driving tree growth across a continental-scale climatic range in Australia. Ecography 44 (7), 1086–1097.
Osakabe, Y., et al., 2014. Response of plants to water stress. Front. Plant Sci. 5, 86.
O, Sungmin., et al., 2022. High-resolution European daily soil moisture derived with machine learning (2003–2020). Sci. Data 9 (1), 1–13.
Pascolini-Campbell, M., 2022. Soil and plants lose more water under drought. Nat. Clim. Change 12 (11), 969–970.
Peng, C., et al., 2011. A drought-induced pervasive increase in tree mortality across Canada's boreal forests. Nat. Clim. Change 1 (9), 467–471.
Pinke, Z., et al., 2022. Changing patterns of soil water content and relationship with national wheat and maize production in Europe. Eur. J. Agron. 140, 126579.
Rezaei, E.E., et al., 2023. Climate change impacts on crop yields. Nature Rev. Earth Environ. 1–16.
Running, S., Mu, Q., Zhao, M. 2015. MOD17A2H MODIS/Terra Gross Primary Productivity 8-Day L4 Global 500m SIN Grid V006 [Data set]. NASA EOSDIS Land Processes Distributed Active Archive Center. Accessed 2023-06-01 from https://doi.org/10.5067/MODIS/MOD17A2H.006.
Running, S., Mu, Q., Zhao, M. 2017. MOD16A2 MODIS/Terra Net Evapotranspiration 8-Day L4 Global 500m SIN Grid V006 [Data set]. NASA EOSDIS Land Processes Distributed Active Archive Center. Accessed 2023-06-08 from https://doi.org/10.5067/MODIS/MOD16A2.006.
Seleiman, M.F., et al., 2021. Drought stress impacts on plants and different approaches to alleviate its adverse effects. Plants 10 (2), 259.
Shapley, L.S., 1953. A value for n-person games. Contribut. Theory of Games 2, 307–317.
Sheridan, S.C., Lee, C.C., 2018. Temporal trends in absolute and relative extreme temperature events across North America. J. Geophys. Res.: Atmos. 123 (21), 11–889.
Sun, C., et al., 2021. Changes in the drought condition over northern East Asia and the connections with extreme temperature and precipitation indices. Global Planet. Change 207, 103645.
Teluguntla, P., et al., 2015. Global Cropland Area Database (GCAD) derived from remote sensing in support of food security in the twenty-first century: current achievements and future possibilities 01–45.
Teshome, A., Zhang, J., 2019. Increase of extreme drought over ethiopia under climate warming. Adv. Meteorol. 1–18.
Thiery, W., et al., 2017. Present-day irrigation mitigates heat extremes. J. Geophys. Res.: Atmos. 122 (3), 1403–1422.
Tijdeman, E., Menzel, L., 2021. The development and persistence of soil moisture stress during drought across southwestern Germany. Hydrol. Earth Syst. Sci. 25 (4), 2009–2025.
Tugwell-Wootton, T., et al., 2020. Soil moisture evaporative losses in response to wet-dry cycles in a semiarid climate. J. Hydrol. 590, 125533.
Vicente-Serrano, S.M., Beguería, S., López-Moreno, J.I., 2010. A multiscalar drought index sensitive to global warming: the standardized precipitation evapotranspiration index. J. Clim. 23 (7), 1696–1718.
Wilhite, D.A., Glantz, M.H., 1985. Understanding: the drought phenomenon: the role of definitions. Water Int. 10 (3), 111–120.
Wilks, D.S., 2011. Statistical Methods in the Atmospheric Sciences. Academic press. Vol. 100.
Xia, et al., 2021. Influences of extreme events on water and carbon cycles of cropland ecosystems: a comprehensive exploration combining site and global modeling. Water Resour. Res. 57 (11).
Xu, K., et al., 2021. Uncertainty assessment of drought characteristics projections in humid subtropical basins in China based on multiple CMIP5 models and different index definitions. J. Hydrol. 600, 126502.
Xu, Z., et al., 2023. Evaluating established deep learning methods in constructing integrated remote sensing drought index: A case study in China. Agric. Water Manage. 286, 108405.
Yang, Y., et al., 2023. Sustainable irrigation and climate feedbacks. Nat Food 4 (8), 654–663.
Yu, Z., et al., 2023. PM2.5 extended-range forecast based on MJO and S2S using LightGBM. Sci. Total Environ. 880, 163358.
Zhang, H., et al., 2023a. Comprehensive evaluation of global precipitation products and their accuracy in drought detection in mainland China. J. Hydrometeorol. 24 (11), 1907–1937.
Zhang, H., Loaiciga, H.A., Sauter, T., 2024. A novel fusion-based methodology for drought forecasting. Remote. Sens. 16 (5), 828.
Zhang, X., et al., 2011. Indices for monitoring changes in extremes based on daily temperature and precipitation data. Wiley Interdiscip. Rev. Clim. Change 2 (6), 851–870.
Zhang, Y., et al., 2023b. Agricultural drought characteristics in a typical plain region considering irrigation, crop growth, and water demand impacts. Agric. Water Manage. 282, 108266.